Supplemental Material can be found at:
http://www.jbc.org/cgi/content/full/M706442200/DC1

THE JOURNAL OF BIOLOGICAL CHEMISTRY VOL. 282, NO. 46, pp. 33859–33867, November 16, 2007
© 2007 by The American Society for Biochemistry and Molecular Biology, Inc. Printed in the U.S.A.

Structure-Function Analysis of the Endoplasmic Reticulum Oxidoreductase TMX3 Reveals Interdomain Stabilization of the N-terminal Redox-active Domain*[S]

Received for publication, August 3, 2007, and in revised form, September 18, 2007 Published, JBC Papers in Press, September 18, 2007, DOI 10.1074/jbc.M706442200

Johannes Haugstetter[‡], Michael Andreas Maurer[‡], Thomas Blicher[§], Martin Pagac[‡1], Gerhard Wider[¶], and Lars Ellgaard[‡2]

From the [‡]Institute of Biochemistry, ETH Zurich, 8093 Zurich, Switzerland, [§]BioCentrum-DTU, Technical University of Denmark, 2800 Lyngby, Denmark, and the [¶]Institute of Molecular Biology and Biophysics, ETH Zurich, 8093 Zurich, Switzerland

Disulfide bond formation in the endoplasmic reticulum is catalyzed by enzymes of the protein disulfide-isomerase family that harbor one or more thioredoxin-like domains. We recently discovered the transmembrane protein TMX3, a thiol-disulfide oxidoreductase of the protein disulfide-isomerase family. Here, we show that the endoplasmic reticulum-luminal region of TMX3 contains three thioredoxin-like domains, an N-terminal redox-active domain (named a) followed by two enzymatically inactive domains (b and b′). Using the recombinantly expressed TMX3 domain constructs a, ab, and abb′, we compared structural stability and enzymatic properties. By structural and biophysical methods, we demonstrate that the reduced a domain has features typical of a globular folded domain that is, however, greatly destabilized upon oxidization. Importantly, interdomain stabilization by the b domain renders the a domain more resistant toward chemical denaturation and proteolysis in both the oxidized and reduced form. In combination with molecular modeling studies of TMX3 abb′, the experimental results provide a new understanding of the relationship between the multidomain structure of TMX3 and its function as a redox enzyme. Overall, the data indicate that in addition to their role as substrate and co-factor binding domains, redox-inactive thioredoxin-like domains also function in stabilizing neighboring redox-active domains.

For many proteins of the secretory pathway and those targeted to the cell surface or secreted, correct folding depends on the formation of native disulfides. The formation of short range disulfide bonds found in some proteins likely requires little catalysis, whereas other proteins rely on the catalyzed formation and rearrangement of disulfides that must be introduced in a nontrivial pattern. The first ER enzyme found to promote these processes was PDI[3] (1). *In vitro*, PDI can catalyze oxidation of free cysteines as well as reduction and isomerization of incorrect disulfide bonds (2–4). It is now clear that a whole family of PDI-like proteins of almost 20 members exists in the mammalian ER (5, 6).

The proteins of the PDI family all contain at least one domain with a thioredoxin fold, where the secondary structure elements are typically arranged as β_1-α_1-β_2-α_2-β_3-α_3-β_4-β_5-α_4. Thioredoxin-like domains that encompass a reactive C*XX*C tetrapeptide sequence are classified as **a**-type domains and otherwise as **b**-type domains. For instance, PDI contains four thioredoxin-like domains named **a**, **b**, **b′**, and **a′**, where **a** and **a′** are redox-active, and **b** and **b′** show no such activity. The redox-active domains generally show a high level of sequence conservation, whereas the **b**-type domains display comparatively little sequence similarity. The function of many **b**-type domains remains unknown. It is clear, however, that the **b′** domain in PDI confers substrate binding (7) and that the corresponding domain in ERp57, the closest homolog of PDI, interacts with the lectin chaperones calnexin and calreticulin that bind glycoprotein substrates (8, 9).

PDI-like proteins with one or more **a**-type domains can oxidize free cysteine residues and reduce disulfides in *in vitro* assays. The same is the case for recombinantly expressed **a**-type domains in isolation (10). However, at least in the case of PDI and ERp57, efficient isomerization requires the presence of one or more **b**-type domains (11–13).

Although PDI and ERp57 are quite well characterized and the crystal structures of *Saccharomyces cerevisiae* PDI (Pdi1p) and a human ERp57 **bb′** construct were recently solved (9, 14), relatively little is known about the cellular functions performed by the human ER oxidoreductases. A plausible explanation for the presence of so many oxidoreductases in the same organelle is that individual PDI homologs interact with discrete or only partially overlapping sets of substrates. An indication that this is indeed the case comes from the recent finding that substrates of ERp57 generally belong to only a subset of glycoproteins characterized by multiple disulfides and a low level of regular secondary structure elements (15).

* This work was supported by ETH Zurich Grant 0-20138-03, Carlsbergfondet, A. P. Møllers Fond til Lægevidenskabens Fremme, and Novo Nordisk Fonden. The costs of publication of this article were defrayed in part by the payment of page charges. This article must therefore be hereby marked "*advertisement*" in accordance with 18 U.S.C. Section 1734 solely to indicate this fact.

[S] The on-line version of this article (available at http://www.jbc.org) contains supplemental Figs. S1–S3.

[1] Present address: Dept. of Medicine/Biochemistry, University of Fribourg, Rue du Musee, 1700 Fribourg, Switzerland.

[2] To whom correspondence should be addressed. Present address: Dept. of Molecular Biology, University of Copenhagen, August Krogh Building, 2100 Copenhagen, Denmark. Tel.: 45-35-32-17-25; Fax: 45-35-32-15-67; E-mail: lellgaard@aki.ku.dk.

[3] The abbreviations used are: PDI, protein disulfide-isomerase; DTT, dithio-1,4-threitol; ER, endoplasmic reticulum; Pdi1p, *S. cerevisiae* PDI; PMSF, phenylmethylsulfonyl fluoride.

Most human PDIs are soluble, but four have a transmembrane region and are grouped in the TMX (thioredoxin-related transmembrane protein) subfamily (5). No substrates are known for the TMX proteins, but it is tempting to speculate that their substrate selectivity is governed by the membrane association. All have a single **a**-type domain facing the ER lumen, except perhaps TMX2, for which the membrane orientation is unclear (16). No experimental characterization has been published for TMX4. The TMX protein has thiol-disulfide exchange activity *in vitro* and can suppress brefeldin A-induced apoptosis when overexpressed (17, 18).

The protein in focus of the current study, TMX3, is expressed in a variety of human tissues, with the highest levels in heart and skeletal muscle (19). The redox state of the active site cysteines in TMX3 is predominantly reduced *in vivo* (19), with ~30% of TMX3 molecules present in the oxidized form (20). Here, we have performed structural, biophysical, and biochemical studies of TMX3 to learn more about the structure-function relations in the protein. Notably, we find that in the three-domain structure of the protein, the redox-active N-terminal domain is stabilized considerably in the context of the full-length protein.

EXPERIMENTAL PROCEDURES

Plasmids and Vectors—pRSET-miniT/TMX3lum (19) was used for the expression of the entire ER luminal region of TMX3 (TMX3lum, residues 25–373; all TMX3 residue numbers in this study refer to the human sequence including the predicted signal peptide, accession number NP_061895). For the expression of TMX3 domain constructs containing one (TMX3 **a**; residues 25–131), two (TMX3 **ab**; residues 25–234), or three domains (TMX3 **abb′**; residues 25–344), the TMX3 cDNA clone hj01608 (KIAA1830 protein) obtained from Kazusa DNA Research Institute served as a PCR template. The forward primer 3-BAB4-Trx-3 (5′-GGGGGATCCAAAGGATTTGTAGAAGATTTAG-3′) was used for all constructs, and the following reverse primers were used to generate TMX3 **a**, TMX3 **ab**, and TMX3 **abb′**, respectively: 4-BAB4-Trx-5 (5′-CCGGAATTCCTACCCAGATACTCTGTGAGCA-3′), 112-TMX3trx2–5 (5′-CCGGAATTCCTACATAGCAAGGTAATTCTG-3′), and 113-TMX3lum Oh-5 (5′-CCGGAATTCCTATACTGTGCCATCCAAAATGTTAT-3′). The PCR products were inserted into the pRSET-miniT expression vector (21) using the BamHI and EcoRI restriction sites to yield pRSET-miniT/TMX3**a**, pRSET-miniT/TMX3**ab**, and pRSET-miniT/TMX3**abb′**. These constructs were used to express domain constructs of TMX3 containing a 17-amino acid N-terminal affinity tag including six consecutive histidines and a thrombin cleavage site. After thrombin cleavage of the affinity tag, a GS dipeptide remains at the N terminus of the TMX3 domain constructs. The sequences of all generated plasmids were verified by DNA sequencing.

Protein Expression and Purification—Protein expression from pRSET-miniT-derived constructs was done as described previously for TMX3lum (19). In brief, the Rosetta(DE3) *Escherichia coli* strain (Novagen) was transformed with expression plasmid and grown in LB medium containing ampicillin and chloramphenicol until an A_{600} of ~0.75 was reached. Protein expression was induced with isopropyl β-D-1-thiogalactopyranoside, and the culture was grown for an additional hour, before the cells were harvested by centrifugation. The ^{15}N-labeled TMX3 **a** was expressed essentially in the same manner, with the exception that the transformed bacteria were grown in Celtone-N complete medium (Spectra Stable Isotopes) instead of LB medium for isotope labeling. The proteins were purified as described previously (19). Briefly, cell pellets were resuspended in buffer containing 6 M guanidine hydrochloride, and the cleared supernatant was then applied onto a Ni^{2+}-charged nitrilotriacetic acid metal affinity chromatography column (Qiagen), refolded while bound on the column by applying a linear gradient into an aqueous buffer, and eluted with a gradient of imidazol-containing aqueous buffer. Fractions containing TMX3 protein were pooled and cleaved with thrombin (Sigma). Finally, the protein was subjected to anion exchange chromatography using a SOURCE15Q column (GE Healthcare), and the purity was assessed by Coomassie staining of SDS-PAGE gels. Protein purification under nondenaturing conditions was done by resuspending the bacterial pellet in a buffer containing 25 mM Tris, pH 8.0, 100 mM NaCl, 5 mM 2-mercaptoethanol, 0.2 mM phenylmethylsulfonyl fluoride (PMSF) followed by cell rupture using a French press. After centrifugation for 45 min at 12,000 × *g*, the cleared supernatants were loaded directly on the affinity chromatography column. Further processing was the same as described above.

Protein Concentration Determination—The concentration of the purified TMX3 proteins was determined from their absorbance at 280 nm by using the molar extinction coefficients calculated by the method of Gill and von Hippel (22). An extinction coefficient of 45,920 M^{-1} cm M was used for TMX3lum and TMX3 **abb′**, 40,800 M^{-1} cm^{-1} for TMX3 **ab**, and 23,590 M^{-1} cm^{-1} for TMX3 **a**.

Limited Proteolysis of TMX3lum—Limited proteolysis was carried out in 10 μM solution of TMX3lum that had been reduced with dithio-1,4-threitol (DTT) prior to dialysis into 100 mM KH_2PO_4/KOH (degassed and flushed with N_2). The reactions were performed at pH 7.0 at 30 °C using the concentrations of trypsin (Sigma), proteinase K (Roche Applied Science), or subtilisin (Roche Applied Science) indicated in Fig. 1. The digests were stopped at various time points by adding PMSF to 10 mM. The samples were analyzed by SDS-PAGE with subsequent Coomassie staining or blotted onto a polyvinylidene fluoride membrane and subjected to N-terminal sequencing. Alternatively, after treatment with PMSF, the samples were separated by size exclusion chromatography on a Superdex S75 HR 10/30 column (GE Healthcare). Fractions containing protein were incubated at 4 °C for 30 min with 0.02% (w/v) deoxycholate and overnight with 10% (w/v) trichloroacetic acid. After centrifugation, the pellets were washed with 70% acetone and analyzed by mass spectrometry (FGCZ Analytical Services, Switzerland).

Analytical Size Exclusion Chromatography—Analytical size exclusion experiments were performed by applying 100 μl of protein sample in 50 mM KH_2PO_4/KOH, pH 7.4, 100 mM NaCl, 1 mM DTT on a Superdex S75 HR 10/30 column that was run at a flow rate of 0.6 ml/min. The results were analyzed by plotting for a set of standard proteins using a low molecular weight gel filtration kit (GE Healthcare), the partition coefficient K_{av},

$$K_{av} = (V_e - V_0)/(V_t - V_0) \quad \text{(Eq. 1)}$$

where V_e is the elution volume, V_0 is the void volume, and V_t is the column volume, against the logarithm of the molecular weight. A linear fit of K_{av} values for the standard proteins then served as a calibration curve to calculate the apparent molecular mass of the TMX3 domain constructs.

CD Measurements—CD measurements were performed on a Jasco J-715 spectropolarimeter in a cell of 1-mm pathlength at 25 °C. The spectra were averaged from 10 scans, and the buffer base line was subtracted. The TMX3 **a** domain was used at a concentration of 27 μM in a buffer containing 50 mM KH_2PO_4/KOH, pH 7.0. The protein was reduced or oxidized by dialyzing overnight against the same buffer containing 0.5 mM DTT or 0.1 mM GSSG, respectively.

NMR Spectroscopy—NMR spectra were measured on a BRUKER DRX600 spectrometer at a proton resonance frequency of 600 MHz using an inverse triple resonance $^{1}H,^{15}N,^{13}C$ probe equipped with an actively shielded z-gradient coil. The 5-mm NMR tubes were filled with 550 ml of a solution of reduced TMX3 **a** domain in 95% H_2O, 5% D_2O containing 50 mM phosphate buffer at pH 8.0. Proton homonuclear one-dimensional spectra and two-dimensional nuclear Overhauser effect spectroscopy spectra (23) were recorded at a temperature of 20 °C. Using the same experimental conditions, a [$^{1}H,^{15}N$]-correlated two-dimensional spectrum (24) was measured on a sample of 0.86 mM ^{15}N-labeled TMX3 **a** domain.

Protein Stability Measurements—Protein stability was measured at different concentrations of ultra pure urea (Sigma) in 100 mM KH_2PO_4/KOH, pH 7.0, 1 mM EDTA, and either 10 mM GSH or 2 mM GSSG using a Varian Cary Eclipse spectrofluorometer. Urea concentrations were determined with a refractometer. Prior to denaturation, the native protein was incubated at room temperature in the presence of 10 mM GSH or 2 mM GSSG for at least 1 h. After adding urea from a concentrated stock solution, the samples were again allowed to equilibrate for 1 h at room temperature, because pilot experiments had demonstrated complete denaturation within this time frame. To test the reversibility of denaturation, samples at the same concentration of urea were produced from native and fully denatured protein, respectively. Pairs of samples generated this way showed nearly identical fluorescence emission spectra. Fluorescence experiments were performed at 25 °C, with a scan rate of 300 nm/min and excitation and emission slits of 5 nm. After excitation at 280 nm, an emission scan was recorded between 300 and 400 nm. Each spectrum was corrected for background fluorescence. The final protein concentration was 0.2 μM. The unfolding profile of each TMX3 domain construct was determined in at least two independent experiments. The presented values were calculated from the experiments shown in Fig. 4.

Data processing was performed as described by Monsellier and Bedouelle (25). Thus, each spectrum was approximated by a Taylor expansion between 320 and 380 nm to the following equation,

$$Y(\lambda,x) \approx a(x) + [(\lambda - \lambda_{max})^2/2!]b(x) + [(\lambda - \lambda_{max})^3/3!]c(x) \quad \text{(Eq. 2)}$$

where Y is the measured fluorescence intensity at the wavelength λ, λ_{max} is the wavelength at which the intensity Y is maximal, x is the urea concentration, $a(x) = Y(\lambda_{max}, x)$, $b(x) = (\delta^2 Y/\delta\lambda^2)(\lambda_{max}, x)$, and $c(x) = (\delta^3 Y/\delta\lambda^3)(\lambda_{max}, x)$, with a, b, c, and λ_{max} as floating parameters.

In the next step, the maximal intensity λ_{max} as a function of the urea concentration x was fitted either to a three-state model

$$\lambda_{max}(x) = [\lambda_N + \lambda_I \exp(-(\Delta G_{NI} - m_{NI}x)/RT) + \lambda_U \exp(-(\Delta G_{NI} - m_{NI}x)/RT)\exp(-(\Delta G_{IU} - m_{IU}x)/RT)]/[1 + \exp(-(\Delta G_{NI} - m_{NI}x)/RT) + \exp(-(\Delta G_{NI} - m_{NI}x)/RT)\exp(-(\Delta G_{IU} - m_{IU}x)/RT)] \quad \text{(Eq. 3)}$$

or to a two-state model

$$\lambda_{max}(x) = [\lambda_N + \lambda_U \exp(-(\Delta G_{NU} - m_{NU}x)/RT)]/[1 + \exp(-(\Delta G_{NU} - m_{NU}x)/RT)] \quad \text{(Eq. 4)}$$

with the floating parameters λ_N, λ_I, and λ_U being the intensity maxima of fluorescence of the native, intermediate, and unfolded state, respectively; ΔG_{NI}, ΔG_{IU}, and ΔG_{NU} are the free energies for the conversions extrapolated to $x = 0$; and m_{NI}, m_{IU}, and m_{NU} are the values for the cooperativity of the respective conversions.

The midpoint of conversion, $x_{1/2}$, *i.e.* the concentration of urea at which $\lambda_{max}(x)$ reached half its maximal value, was calculated as follows.

$$x_{1/2} = \Delta G/m \quad \text{(Eq. 5)}$$

Because the recorded value of $\lambda_{max}(x)$ is not a linear function of the molar fractions of the folded and unfolded states, $x_{1/2}$ does not represent half-advancement of the unfolding reaction. Hence, the midpoint of denaturation, $x'_{1/2}$, was calculated by introducing a corrective term as detailed in Ref. 25.

Peptide Oxidation Assay—The ability of TMX3 domain constructs to oxidize dithiols was investigated by following the fluorescence change upon oxidation of the decapeptide NRCSQGSCWN, as described earlier (19). Data analysis was performed as detailed in Ref. 26.

Reaction Kinetics of TMX3 Domain Constructs with GSSG—Pseudo first order rate constants and apparent second order rate constants for the reaction between reduced TMX3 domain constructs and GSSG were determined by measuring the fluorescence change upon oxidation of the protein essentially as described in Ref. 27. Proteins used in this assay were reduced for 1 h at room temperature with 2 mM DTT before the reducing agent was removed on a Micro Bio-Spin 30 column (Bio-Rad), pre-equilibrated in 50 mM Tris, pH 7.0, 50 mM NaCl, 1 mM EDTA (degassed and flushed with N_2). Finally, protein samples were diluted to ~0.25 μM in the same buffer. Fluorescence emission at 328 nm, upon excitation at 280 nm, was then monitored in a stirrable quartz cuvette that had been silanized to minimize adsorption to the glass surface, as observed in particular for the TMX3 **a** domain upon oxidation. After a stable base line was attained, the reaction was initiated by the addition of a molar excess of GSSG (final concentrations, 16-355 μM) from a

concentrated stock solution. Pseudo first order rate constants were determined by fitting single exponential functions to the data points. In particular for TMX3 **a**, we observed a drop in the fluorescence signal when full oxidation was approached, most likely because of glass adsorption as mentioned above. In these cases, we only included data points for the fit corresponding to ~90% completion of oxidation. An apparent second order rate constant was determined from a linear fit to a series of experiments with varying GSSG concentrations. Two sets of independent experiments were performed with similar results.

Molecular Modeling—A working model of TMX3 **abb′** was constructed with the program Modeller (28) using default settings and the alignment shown in supplemental Fig. S1. The model comprises residues 25–340 and is based on the NMR solution structure of the PDI **a** domain (Protein Data Bank code 1MEK) (29) for TMX3 **a** and the crystal structure of rabbit skeletal muscle calsequestrin (Protein Data Bank code 1A8Y) (30) for the TMX3 **bb′** region. When constructing the model, an overlapping and similar region between the two templates was included in the alignment. This way the templates were aligned to preserve the relative domain orientation in calsequestrin.

The quality of the model was assessed by submitting it to the ProQ server (www.sbc.su.se/~bjornw/ProQ/), which has been designed to evaluate protein homology models (31). The evaluation produced scores that were indicative of a reliable, high quality model (LGscore = 4.09, MaxSub = 0.48). Analysis of the backbone dihedral angles in the model using the MolProbity server (molprobity.biochem.duke.edu/) (32) showed that 94% of the residues were in the most favored regions, and 99% were within allowed regions. Only three outliers (Leu^{68}, Pro^{116}, and Ser^{139}) were marginally outside the allowed regions. Overall, this is comparable with the quality of the NMR template (PDI **a**).

RESULTS

Determination of Domain Boundaries in the Luminal Region of TMX3—To analyze the domain composition of TMX3 and the relative stability of domains toward proteolysis, we subjected the recombinant full-length luminal region (TMX3lum; residues 25–373 (19)) to limited proteolysis. After digestion with subtilisin, proteinase K, or trypsin, digest mixtures were separated by SDS-PAGE (Fig. 1) and transferred onto a polyvinylidene fluoride membrane from which single bands were excised and subjected to N-terminal sequencing. Alternatively, digest mixtures were separated by size exclusion chromatography and then analyzed by mass spectrometry. The fragments identified by these methods are listed in Table 1, where the numbering corresponds to the labeling of bands on the SDS-PAGE gel shown in Fig. 1*B*. A schematic overview of the fragments obtained with respect to their position in the TMX3 sequence is depicted in Fig. 1*C*.

The luminal region of TMX3 harbors an N-terminal thioredoxin-like domain that shows 38% sequence identity to the PDI **a** domain and contains a CGHC active site sequence (see Fig. 3*B*). This domain comprises residues 25–131 of TMX3 as indicated by sequence alignments with PDI, ERp57, and other ER oxidoreductases. Indeed, all three proteases cleaved TMX3lum close to residue 131 (fragments 4, 7, and 11).

The remaining two thirds of TMX3lum are weakly similar to calsequestrin, a calcium-binding protein containing three redox-inactive thioredoxin-like domains. In TMX3lum, cleavage sites clustered in two areas in the C-terminal region: residues 225–235 (fragments 3, 4, 6, 7, and 10) and near residue 355 close to the C terminus (fragments 1, 5, and 8). In the case of

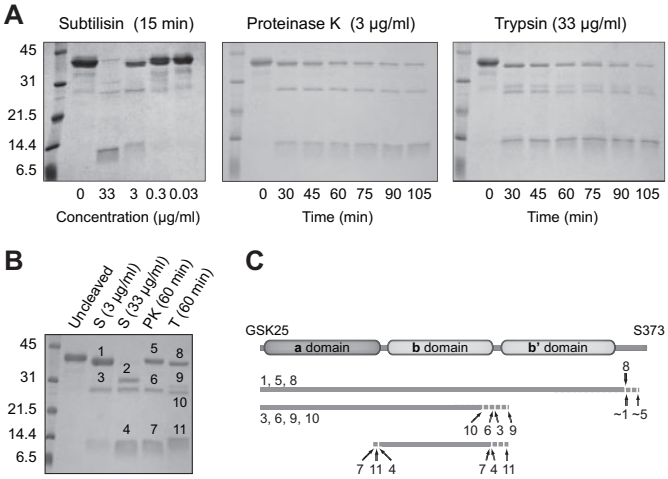

FIGURE 1. **Limited proteolysis of the luminal region of TMX3.** *A*, recombinantly expressed TMX3lum was digested with the indicated proteases at various concentrations and/or for different periods of time. The digests were stopped by adding PMSF and separated by SDS-PAGE, and the gels were stained with Coomassie blue. *B*, overview of fragments generated under specific proteolytic conditions and selected for further analysis by N-terminal sequence analysis and mass spectrometry. The numbering of fragments corresponds with that in Table 1 and Fig. 1*C*. *S*, subtilisin; *PK*, proteinase K; *T*, trypsin. For all gels the first lane shows a molecular mass marker with the individual bands labeled in kDa next to the gel. *C*, domain organization of TMX3. The schematic representation of TMX3lum (residues Lys^{25}–Ser^{373}) at the *top* shows the three thioredoxin-like domains **a** (*dark gray*) and **b** and **b′** (*light gray*) as *oval boxes*. The nonnative GS dipeptide at the N terminus appears as a result of the cloning strategy for recombinant expression of the protein. The identified proteolytic fragments of TMX3lum are shown below the schematic representation of the protein. The *numbers* refer to the fragments listed in Table 1, and the positions of cleavage sites are indicated by *arrows*. For a mapping of the domain boundaries onto the TMX3 sequence and in relation to predicted secondary structure elements, see supplemental Fig. S1.

TABLE 1

N-terminal sequences and mass spectrometric analysis of fragments from limited proteolysis of TMX3lum

Proteolytic fragments of TMX3lum generated by subtilisin, proteinase K, and trypsin were subjected to N-terminal sequencing and mass spectrometric analysis. The numbering of fragments corresponds to the numbering of bands in Fig. 1*B*, whereas sequence numbers under Fragment identity refer to human full-length TMX3 (accession number NP_061895). Note that recombinant TMX3 contains a nonnative GS dipeptide at its N terminus. ND, not determined.

Fragment number	Protease	N-terminal sequence	Mass	Fragment identity
			Da	
TMX3lum	Untreated	GSKG	40,385	25–373
1	Subtilisin	GSKGF	ND	25–?
2	Subtilisin	ND	27,850	ND
3	Subtilisin	GSKG	24,676	25–235
4	Subtilisin	GALI	12,233	131–233
5	Proteinase K	GSKG	ND	25–?
6	Proteinase K	GSKG	24,532	25–234
7	Proteinase K	AHRV	12,780	126–232
8	Trypsin	GSKG	38,409	25–355
9	Trypsin	GXK	26,016	25–247
10	Trypsin	GSKG	23,455	25–225
11	Trypsin	VSGA	13,950	129–247

subtilisin, the short C-terminal fragment was removed even at low concentrations of protease where smaller stable fragments were not yet generated (Fig. 1*A*), indicating it to be a highly accessible flexible tail.

Overall, the results indicated that TMX3 contained three structural entities of about the same size. Secondary structure predictions (33) were consistent with the presence of two thioredoxin-like domains in TMX3 in addition to the N-terminal redox-active domain (supplemental Fig. S1). Moreover, the protease cleavage sites clustered in three distinct regions that correlated well with the expected positions of interdomain linkers and the sequence region between the most C-terminal domain and the transmembrane domain (supplemental Fig. S1). In accordance with common practice, the three thioredoxin-like domains in TMX3 were named **a**, **b**, and **b′**.

These experiments also provided information about the relative stability of the different domains toward proteolysis. The only single domain detected was the **b** domain (fragments 4, 7, and 11). Four fragments comprised the **ab** double domain (fragments 3, 6, 9, and 10). Contrary to this, fragments containing the TMX3 **bb′** double domain were not detected. We concluded that the TMX3 **b** domain was most resistant toward proteolytic degradation and that upon the fast removal of the C-terminal tail the **b′** domain is degraded. Apparently the **b** domain provides significantly higher protection against proteolysis for the **a** domain than for the **b′** domain, indicating a role for the **b** domain in interdomain stabilization of the **a** domain.

Expression and Gel Filtration Analysis of TMX3 Domain Constructs—For further experiments, we used TMX3 constructs comprising the **a** domain (residues 25–131), the **ab** domains (residues 25–234), or all three domains (**abb′**, residues 25–344). The domain boundaries were based on the results of the proteolysis experiments, as well as sequence alignments and secondary structure predictions that indicated the constructs to contain all regular secondary structure elements of a canonical thioredoxin fold (Fig. 3*B* and supplemental Fig. S1).

The purification protocol involved protein solubilization in a denaturing buffer followed by refolding on an affinity chromatography column and anion exchange chromatography. This protocol was employed because of its higher yields after having ensured that the refolded TMX3 **a** and **ab** constructs, initially purified under native conditions, showed no differences by CD or fluorescence spectroscopy to the natively purified proteins (data not shown). Likewise, no other experiments such as NMR spectroscopy and stability measurements (where reversibility of unfolding was demonstrated) gave reason to believe that refolding resulted in perturbations of the native structure.

The homogeneity of the purified TMX3 domain constructs was assessed by SDS-PAGE (Fig. 2*A*) and analytical size exclusion chromatography (Fig. 2*B*). The apparent and theoretical masses were in good agreement for all TMX3 domain constructs, indicating that all are likely to be spherically shaped proteins. No evidence for oligomerization was observed.

*NMR Spectroscopic Analysis and Molecular Modeling of the TMX3 **a** Domain*—As a starting point for a more detailed structure-function analysis, we chose the redox-active TMX3 **a** domain. For NMR structural investigations, unlabeled and ^{15}N-labeled protein samples were generated and used to measure

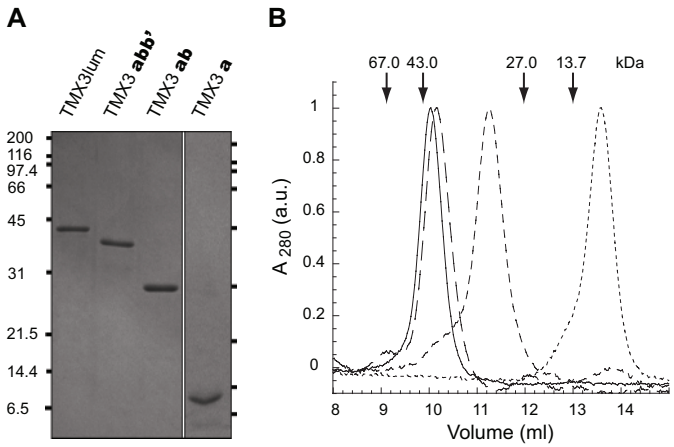

FIGURE 2. **Purification and analytical size exclusion chromatography of TMX3 domain constructs.** *A*, in addition to TMX3lum, fragments comprising **a**, **ab**, or **abb′** were recombinantly expressed in *E. coli* and purified. The homogeneity of all purified TMX3 fragments was assessed by SDS-PAGE. The *marks* on the side of each Coomassie-stained gel show the position and size (in kDa) of molecular mass marker bands. *B*, elution profiles of TMX3lum (*solid line*) and the **a** (*dotted line*), **ab** (*short dashed line*), and **abb′** (*long dashed line*) domain constructs from a calibrated Superdex S75 HR column. Individual elution profiles were scaled to adjust all the peaks to the same height. Based on the elution volumes of marker proteins (indicated by *arrows*), apparent masses were calculated for the TMX3 domain constructs. Those consisting of more than one domain tended to have slightly larger apparent masses (TMX3lum, 46.0 kDa; TMX3 **abb′**, 43.9 kDa; TMX3 **ab**, 28.5 kDa) compared with their theoretical masses (40.4, 37.2, and 24.6 kDa, respectively), whereas the apparent mass of the TMX3 **a** domain (11.7 kDa) was very close to its theoretical mass (12.3 kDa). The deviation of the apparent masses from the theoretical masses was in the same range as the difference from the linear calibration fit observed for the individual proteins used for the calibration, indicating spherical shapes for all TMX3 constructs. *a.u.*, arbitrary units.

one-dimensional and two-dimensional NMR spectra under reducing conditions. The proton one-dimensional spectrum displayed the features expected for a folded globular protein; several methyl and amide proton resonances were shifted well out of the bulk of the spectrum that had line widths expected for the size of TMX3 **a** (data not shown). For a more detailed characterization we measured a ^{1}H,^{15}N correlation spectrum of ^{15}N-labeled reduced TMX3 **a** (Fig. 3*A*). In well structured proteins each backbone amide group, except the N-terminal one, is expected to be represented by one peak in this type of spectrum. Indeed, this is exactly what was observed, demonstrating that the whole protein is NMR-detectable. Moreover, the resonances were well dispersed, indicating a globular folded protein containing α-helical and β-sheet secondary structure elements and only few residues in unstructured parts. A proton homonuclear two-dimensional nuclear Overhauser effect spectroscopy spectrum confirmed the impression of the other two spectra because the resonances were well dispersed in the two-dimensional plane, and the clustering of resonances typical for unfolded proteins was not seen (data not shown).

We also built a structural model of the TMX3 **abb′** fragment as described under "Experimental Procedures" and shown in its entirety in supplemental Fig. S2. Based on the 38% sequence identity and the predicted conservation of the positions of individual regular secondary structure elements between TMX3 **a** and PDI **a** (Fig. 3*B*), the model of the **a** domain is likely quite reliable. With a number of residues expected to play a role in catalysis conserved between the two proteins (Fig. 3*B*), we

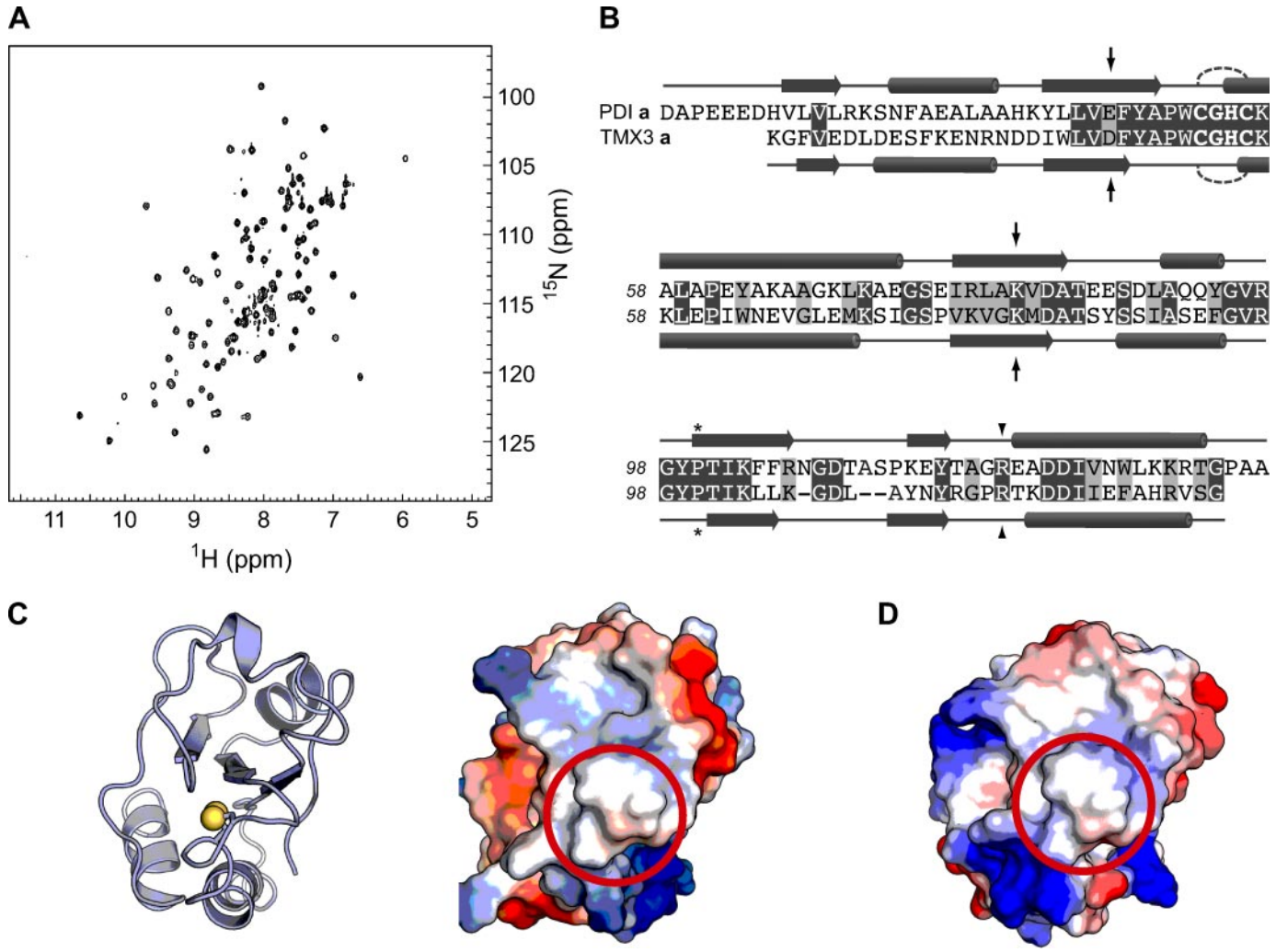

FIGURE 3. **NMR spectroscopic characterization and molecular modeling of the TMX3 a domain.** *A*, contour plot of a two-dimensional NMR ^{1}H,^{15}N correlation spectrum of reduced, ^{15}N-labeled TMX3 **a** measured at 600 MHz. The concentration was 0.86 mM at pH 8.0, and the measurement temperature was 20 °C. *B*, sequence alignment between human PDI **a** and TMX3 **a**. The *black boxes* show amino acid identities, and the *gray boxes* show amino acid similarities. Experimentally determined secondary structure elements of the PDI **a** NMR structure and predicted secondary structure elements in TMX3 **a** are shown (helices and strands are represented by *cylinders* and *arrows*, respectively). The prediction was performed using the JPRED algorithm. Active site residues are in *bold face type*. A number of conserved residues important for catalysis are marked: *black arrows* indicate a charge pair (Asp^{47}/Lys^{81}) involved in proton-transfer reactions, the *asterisk* indicates a proline residue (Pro^{100}) that usually forms a *cis*-Pro loop, and the *arrowhead* indicates an arginine residue (Arg^{117}) proposed to influence the pK_a of the active site cysteines (14, 42). *C*, ribbon diagram with active site cysteines depicted as *yellow spheres* (*left*) and electrostatic surface plot (*right*) of the PDI **a** NMR structure shown in the same orientation. *Red* illustrates an overall negative charge, *blue* shows a positive charge, and *white* is uncharged. *D*, electrostatic surface plot of the modeled TMX3 **a** domain shown in the same orientation as PDI **a** in the previous panel. In *C* and *D* the hydrophobic patch in the vicinity of the active site is *encircled*. The molecular graphics were prepared with PyMol (43).

focused our attention on the surface properties of TMX3 **a**. A hydrophobic patch is apparent around the active site cysteines, whereas the rest of the surface is covered with polar or charged residues (Fig. 3*D*). A similar pattern is seen for human PDI **a** (Fig. 3*C*) (29) and other oxidoreductases such as Pdi1p **a** and **a′** (14), human and barley thioredoxin (34, 35), and DsbA (36). The hydrophobic patch likely interacts with short stretches of unfolded polypeptide chains in substrate proteins.

*Far UV CD Spectroscopic Analysis of Reduced and Oxidized TMX3 **a***—We next studied the secondary structure content of TMX3 **a** by far UV CD spectroscopy under both reducing and oxidizing conditions (Fig. 4*A*). In accordance with the NMR data, the CD spectrum of reduced TMX3 **a** showed that the protein is well structured and contains both α-helices and β-sheets, as expected for a typical thioredoxin-like domain. However, upon oxidation, the negative maximum was blue-shifted and became less intense, indicating a conformational change with appreciable contribution from random coil conformation. A similar conformational change upon oxidization has previously been observed by CD spectroscopy for the PDI **a′** domain (11) but not for ERp57 **a** and **a′** (13).

Chemical Denaturation of TMX3 a, ab, and abb′—To learn more about the structural stability of the protein, we performed urea unfolding studies on all three domain constructs under reducing and oxidizing conditions. Fluorescence spectroscopy was used to follow the structural changes upon denaturation. After excitation at 280 nm, an emission spectrum was recorded between 300 and 400 nm, and the experimentally determined values of λ_{max}, the wavelength of maximal intensity, were plotted *versus* the concentration of urea and fitted to obtain the midpoint of conversion, $x_{1/2}$. This value, however, does not represent half-advancement of the unfolding reaction because the

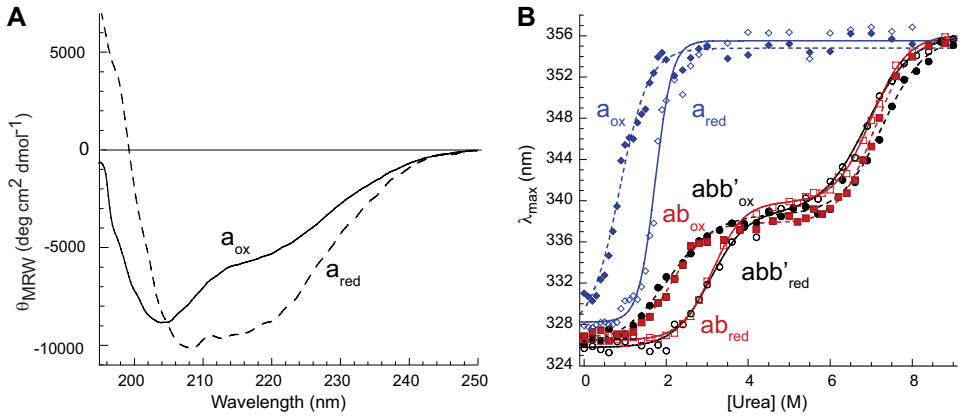

FIGURE 4. **Stability measurements of reduced and oxidized TMX3 fragments.** *A*, far UV CD spectra of reduced (*dashed line*) and oxidized (*solid line*) TMX3 **a**. The protein was either reduced with 0.5 mM DTT or oxidized with 0.1 mM GSSG. *B*, 0.2 μM of TMX3 **a** (*blue diamonds*), TMX3 **ab** (*red squares*), or TMX3 **abb′** (*black circles*), were reduced in the presence of 10 mM GSH (*empty symbols*) or oxidized in the presence of 2 mM GSSG (*filled symbols*) and subsequently denatured with urea. After excitation at 280 nm, fluorescence emission spectra were recorded between 300 and 400 nm. Each spectrum was background corrected, and the wavelength values at which maximal fluorescence emission was observed, λ_{max}, were plotted in dependence of the urea concentration. The data points were fitted to a two-state model (TMX3 **a**) or a three-state model (TMX3 **ab** and TMX3 **abb′**) to obtain the midpoints of conversion $x_{1/2}$. Note that the midpoints of denaturation, $x'_{1/2}$, given in the text were calculated by introducing a corrective term to compensate for the nonlinear relationship between the λ_{max} signal and the concentrations of native and denatured protein, which is why they are not exactly the same values that can be determined by visual inspection of the curves in this panel.

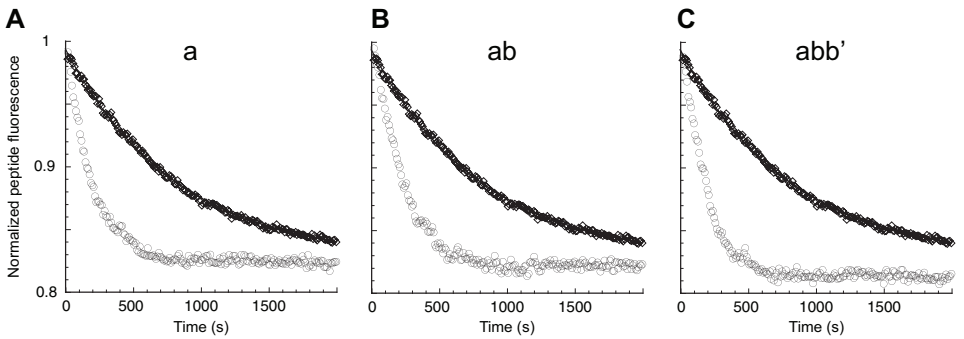

FIGURE 5. **Comparison of peptide oxidation by TMX3 fragments.** Shown is the time-dependent fluorescence change of the peptide NRCSQGSCWN upon oxidation. The data were recorded at 350 nm after excitation at 280 nm. The normalized peptide fluorescence given on the ordinate was obtained by normalizing to the value of the fully reduced peptide after subtraction of the protein fluorescence. The reaction was performed in 100 mM KH_2PO_4/KOH, pH 7.0, 2 mM EDTA, 2 mM GSH, and 0.5 mM GSSG with 3.4 μM peptide substrate, and oxidation was catalyzed by 0.2 μM protein and compared with the uncatalyzed reaction. The half-times for oxidation were determined to be 166 ± 25 s for TMX3 **a** (o, *A*), 142 ± 31 s for TMX3 **ab** (o, *B*), 151 ± 32 s for TMX3 **abb′** (o, *C*), and 607 ± 48 s for the uncatalyzed reaction (◇, *A–C*). In the case of the uncatalyzed reaction, the exponential fit shown was used to derive the half-time, whereas the corresponding values for the TMX3 fragments were obtained as described by Ruddock *et al.* (26).

recorded value of λ_{max} is not a linear function of the molar fractions of the folded and unfolded states. The true midpoints of denaturation, $x'_{1/2}$, given in the text were calculated by introducing a corrective term to compensate for the nonlinearity (25), which is why they are not exactly equivalent to the values obtained by visual inspection of the curves in Fig. 4*B*.

Upon fitting the λ_{max} values recorded for the TMX3 **a** domain to a two-state model, midpoints of denaturation for the reduced and oxidized states of ~1.3 and 0.4 M urea, respectively, were calculated (Fig. 4*B*, *blue curves*). The partial loss of secondary structure observed even in the absence of urea for the oxidized state (Fig. 4*A*) correlates well with the low stability detected by chemical denaturation. For the TMX3 **ab** and **abb′** constructs, two unfolding steps were observed, and the λ_{max} values in dependence of the urea concentration were best fitted to a three-state model. As seen for the **a** domain in isolation, the first unfolding step was found to be sensitive to the oxidation state. However, with the higher stability evidently offered by the **b** and **bb′** domains, the denaturation midpoint shifted to ~2.3 M urea under reducing conditions and ~1.6 M urea for the oxidized state. The second unfolding step, which we attribute to the **b** domain, was independent of the redox state and took place at ~7 M urea.

*Peptide Oxidation Activity of TMX3 **a**, **ab**, and **abb′***—Considering the different structural and biophysical properties of the TMX3 domain constructs, we decided to compare their redox activity. The catalytic activity of TMX3 **a**, **ab**, and **abb′** was investigated by comparing their ability to oxidize a model peptide containing two cysteines (26). In this peptide, the formation of an intramolecular disulfide quenches the intrinsic fluorescence of a tryptophan residue to 81% when compared with the reduced peptide. Here, we added 0.2 μM protein to 3.4 μM reduced peptide substrate in a buffer with a neutral pH containing 2 mM GSH and 0.5 mM GSSG and monitored the progress of the reaction by fluorescence spectroscopy (Fig. 5). The reaction profiles all fit well to an exponential function with random residuals indicating the reaction to be first order toward substrate and thereby peptide oxidation to be rate-limiting (10) (see also supplemental Fig. S3). When previously performing this assay, we found reaction half-times of 270 s for TMX3lum and 80 s for PDI (19). Here, we found all three domain constructs of TMX3 to be faster catalysts than the entire luminal domain with reaction half-times of ~150 s.

Determination of the Rate Constants for the Reaction between Reduced TMX3 Domain Constructs and GSSG—Finally, we determined the kinetics of the reaction between reduced TMX3 domain constructs and GSSG. We used a fluorescence-based assay taking advantage of the observation that upon excitation at 280 nm, TMX3 **a**, **ab**, and **abb′** all showed ~1.3 times higher fluorescence emission at 328 nm in the reduced compared with the oxidized state (data not shown). Pseudo first order rate constants were obtained from fitting a single-exponential function to the fluorescence change of reduced TMX3

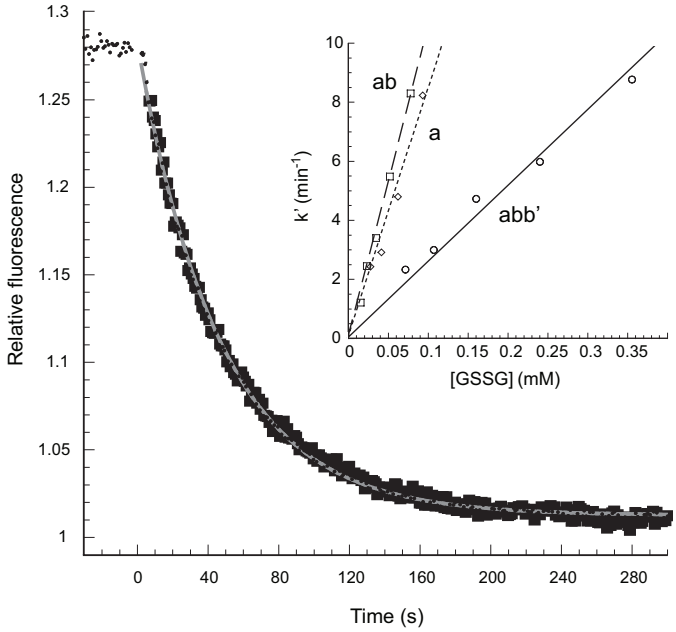

FIGURE 6. **Determination of rate constants for the reaction between reduced TMX3 domain constructs and GSSG.** The reaction between 0.25 μM TMX3 **ab** and 16 μM GSSG in 100 mM potassium phosphate at pH 7.0 and 1 mM EDTA at 25 °C was monitored by following the change in fluorescence at 328 nm upon excitation at 280 nm. A pseudo first order rate constant $k' = 1.2$ min^{-1} was obtained by fitting a single exponential function to the data points. *Inset*, plot of the pseudo first order rate constants, k', obtained from a series of equivalent experiments by varying [GSSG] between 16 and 355 μM, against [GSSG]. Linear fits yielded apparent second order rate constants of 84 mM^{-1} min^{-1} for TMX3 **a** (*diamonds*, *dotted line*), 105 mM^{-1} min^{-1} for TMX3 **ab** (*squares*, *dashed line*), and 26 mM^{-1} min^{-1} for TMX3 **abb′** (*circles*, *solid line*).

domain constructs (~0.25 μM) upon mixing with a molar excess of GSSG (16–355 μM). As an example, the reaction of TMX3 **ab** with 16 μM GSSG is shown in Fig. 6. From a series of reactions performed at varying concentrations of GSSG, apparent second order rate constants (k_{app}) were determined. As illustrated in Fig. 6 (*inset*), the k_{app} values obtained with the TMX3 **a** and **ab** constructs (105 mM^{-1} min^{-1} and 84 mM^{-1} min^{-1}, respectively) were faster than the value of 26 mM^{-1} min^{-1} for the TMX3 **abb′** construct.

DISCUSSION

In the multi-domain proteins of the PDI family, a particular combination of redox-active and noncatalytic thioredoxin-like domains seems to be critical to ensure the specificity for distinct types of substrates. Moreover, noncatalytic domains in different enzymes must be able to fulfill different functions. Here, we have shown that TMX3 is composed of one redox-active domain (**a**) and two noncatalytic domains (**b** and **b′**). In addition, a roughly 30-residue linker sequence connects the **b′** domain to the transmembrane region of the protein. This linker is predicted to form an amphipathic helix from Ile^{352} to Phe^{371}. Because this sequence is located immediately N-terminal to the transmembrane region, which is predicted to start at Pro^{375}, it might well mediate membrane association.

For the isolated TMX3 **a** domain, oxidation of the active site disulfide resulted in partial unfolding and destabilization. Judging by the CD spectra (Fig. 4*A*), a quite substantial conformational change takes place upon oxidation. Unfortunately, we could not characterize this change in more detail because we were unable to produce the oxidized **a** domain at the concentration needed for recording a ^{1}H,^{15}N correlation spectrum because of problems of aggregation.

For TMX3 **ab** and **abb′**, denaturation studies revealed two separate transitions (Fig. 4*B*). The first likely reflects the denaturation of the **a** domain because it was clearly stabilized in the reduced **ab** and **abb′** constructs. Moreover, the presence of **b** and **bb′** notably stabilized the **a** domain regardless of its redox state (compare *red* and *black curves* with *blue curves* in Fig. 4*B*). The second transition represents the unfolding of the **b** domain. Because of the absence of tryptophan residues in TMX3 **b′**, its unfolding could not be followed by fluorescence spectroscopy. However, the presence of the **b′** domain did not influence the stability of either transition. The results of the denaturation experiments correlated well with the proteolysis studies that revealed the **b** domain to be most protease-resistant and to have a protective effect on the **a** domain toward protease digestion.

Particularly for the oxidized domain constructs, the conventional use of fluorescence intensity in dependence of the denaturant concentration to calculate protein stability turned out not to be ideal. Likely because of protein aggregation and/or adsorption to the glass cuvette of oxidized TMX3 fragments, the intensity data scattered more than the wavelength maximum data used instead. This method gave a robust signal that had the advantage of being concentration-independent. Although the relationship between λ_{max} and the fractions of folded and unfolded protein is not linear, the method reliably determines transition midpoints (25). Primarily because certain pretransition regions, especially that of the oxidized **a** domain, were too short to obtain nearly perfect fits, we did not use the thermodynamic stabilities, ΔG values, as quantitative measures of protein stability. Although transition midpoints are not exact representations of protein stability, they did allow valid semi-quantitative estimates to be made. Because the conclusions about the relative stabilities are independent of the exact numbers, the urea concentrations at midpoint served well as a measure of protein stability when comparing the TMX3 domain constructs.

The enzymatic characterization revealed that all TMX3 domain constructs catalyzed the oxidation of a model peptide faster than TMX3lum (19). Because of the partial hydrophobic nature of the C-terminal tail present in the TMX3lum construct, it is conceivable that this region can compete for binding of the peptide substrate by interaction with the hydrophobic patch close to the active site in the **a** domain.

The TMX3 **abb′** construct was oxidized a bit slower by GSSG than TMX3 **a** and **ab** (Fig. 6, *inset*; experiment performed at pH 7.0). The differences that we observed between TMX3 **ab** and TMX3 **abb′** in peptide oxidation kinetics at concentrations of GSSG below ~250 μM (see supplemental Fig. S3) were in full agreement with the finding that TMX3 **ab** reacted faster than TMX3 **abb′** with GSSG. Although it is presently unclear why TMX3 **abb′** was oxidized slower than the two shorter domain constructs, it is interesting to note that the k_{app} values determined here for the TMX3 constructs were all in the range reported for the PDI **a** and **a′** domains of ~36 mM^{-1} min^{-1} at

pH 7.4 (37). For comparison, these values are approximately 3 orders of magnitude faster than the reaction of GSSG with the cysteine pair in the rxYFP redox sensor (k_{app} = 0.072 mM^{-1} min^{-1} at pH 7.0) (27). Given their very similar redox potentials (19, 37, 38), the results indicate that TMX3 and PDI will equilibrate approximately equally fast with the glutathione redox buffer in the ER lumen.

Based on the NMR structure of human PDI **a** and the crystal structure of rabbit skeletal muscle calsequestrin, we built a structural model of TMX3 **abb′** (supplemental Fig. S2). In this model, the relative domain orientations are imposed by the calsequestrin template. The quite short linker lengths between domains in TMX3 (supplemental Fig. S1) are similar to those also seen in calsequestrin, Pdi1p, and other family members (39). This feature must limit the degrees of freedom between the **a** and **b** domains and between the **b** and **b′** domains, respectively. As noted previously (14), it is striking how well the thioredoxin domains of calsequestrin align structurally with the **abb′** domains of Pdi1p. By conjecture, but presently quite speculative, the domain orientations in TMX3 could be similar to those in Pdi1p **abb′** as suggested by supplemental Fig. S2. No hydrophobic surface regions at the interface between the **a** and **b** domains were observed in the TMX3 model, and the molecular details of how the **b** domain stabilizes the **a** domain await further structural studies.

Previously, it has been hypothesized that the PDI **a′** domain, which partially unfolds upon oxidation, would be stabilized in the context of the entire protein (11). Here, we clearly show that such a mechanism is indeed in place for the TMX3 **a** domain, where pronounced effects were observed as a result of interdomain stabilization by the **b** domain. Our results therefore indicate that at least certain PDI family members capable of catalyzing oxidation might rely on noncatalytic domains for structural stabilization. The destabilization of **a**-type domains observed upon oxidation in TMX3 and PDI is a feature found to correlate with efficient transfer of the active site disulfide in other oxidoreductases, *e.g.* DsbA (40). Whether TMX3 and PDI act as efficient catalysts of protein oxidation *in vivo* is still an open question; so far, the only proposed substrate of the flavin-binding oxidase ER oxidase 1 in mammalian cells is PDI (41). We are currently investigating this point further for both PDI and TMX3.

Acknowledgments—We thank the Institute of Biochemistry, ETH Zurich, for the continued support, Rudi Glockshuber for helpful suggestions, and Karen Skriver, Jakob R. Winther, and all members of the Ellgaard lab for critical reading of the manuscript. The peptide for the oxidation assay was kindly provided by Lloyd W. Ruddock.

REFERENCES

1. Givol, D., Goldberger, R. F., and Anfinsen, C. B. (1964) *J. Biol. Chem.* **239,** PC3114–3116
2. Creighton, T. E., Hillson, D. A., and Freedman, R. B. (1980) *J. Mol. Biol.* **142,** 43–62
3. Weissman, J. S., and Kim, P. S. (1993) *Nature* **365,** 185–188
4. Darby, N. J., Freedman, R. B., and Creighton, T. E. (1994) *Biochemistry* **33,** 7937–7947
5. Ellgaard, L., and Ruddock, L. W. (2005) *EMBO Rep.* **6,** 28–32
6. Sevier, C. S., and Kaiser, C. A. (2006) *Antioxid. Redox. Signal.* **8,** 797–811
7. Klappa, P., Ruddock, L. W., Darby, N. J., and Freedman, R. B. (1998) *EMBO J.* **17,** 927–935
8. Russell, S. J., Ruddock, L. W., Salo, K. E., Oliver, J. D., Roebuck, Q. P., Llewellyn, D. H., Roderick, H. L., Koivunen, P., Myllyharju, J., and High, S. (2004) *J. Biol. Chem.* **279,** 18861–18869
9. Kozlov, G., Maattanen, P., Schrag, J. D., Pollock, S., Cygler, M., Nagar, B., Thomas, D. Y., and Gehring, K. (2006) *Structure* **14,** 1331–1339
10. Alanen, H. I., Salo, K. E., Pirneskoski, A., and Ruddock, L. W. (2006) *Antioxid. Redox. Signal.* **8,** 283–291
11. Darby, N. J., and Creighton, T. E. (1995) *Biochemistry* **34,** 11725–11735
12. Darby, N. J., Penka, E., and Vincentelli, R. (1998) *J. Mol. Biol.* **276,** 239–247
13. Frickel, E. M., Frei, P., Bouvier, M., Stafford, W. F., Helenius, A., Glockshuber, R., and Ellgaard, L. (2004) *J. Biol. Chem.* **279,** 18277–18287
14. Tian, G., Xiang, S., Noiva, R., Lennarz, W. J., and Schindelin, H. (2006) *Cell* **124,** 61–73
15. Jessop, C. E., Chakravarthi, S., Garbi, N., Hämmerling, G. J., Lovell, S., and Bulleid, N. J. (2007) *EMBO J.* **26,** 28–40
16. Meng, X., Zhang, C., Chen, J., Peng, S., Cao, Y., Ying, K., Xie, Y., and Mao, Y. (2003) *Biochem. Genet.* **41,** 99–106
17. Matsuo, Y., Akiyama, N., Nakamura, H., Yodoi, J., Noda, M., and Kizaka-Kondoh, S. (2001) *J. Biol. Chem.* **276,** 10032–10038
18. Matsuo, Y., Nishinaka, Y., Suzuki, S., Kojima, M., Kizaka-Kondoh, S., Kondo, N., Son, A., Sakakura-Nishiyama, J., Yamaguchi, Y., Masutani, H., Ishii, Y., and Yodoi, J. (2004) *Arch. Biochem. Biophys.* **423,** 81–87
19. Haugstetter, J., Blicher, T., and Ellgaard, L. (2005) *J. Biol. Chem.* **280,** 8371–8380
20. Appenzeller-Herzog, C., and Ellgaard, L. (2007) *Antiox. Redox. Signal.*, **10,** 10.1089/ars.2007.1837
21. Zahn, R., Buckle, A. M., Perrett, S., Johnson, C. M., Corrales, F. J., Golbik, R., and Fersht, A. R. (1996) *Proc. Natl. Acad. Sci. U. S. A.* **93,** 15024–15029
22. Gill, S. C., and von Hippel, P. H. (1989) *Anal. Biochem.* **182,** 319–326
23. Kumar, A., Ernst, R. R., and Wuthrich, K. (1980) *Biochem. Biophys. Res. Commun.* **95,** 1–6
24. Bodenhausen, G., and Ruben, D. J. (1980) *Chem. Phys. Lett.* **69,** 185–189
25. Monsellier, E., and Bedouelle, H. (2005) *Protein. Eng. Des. Sel.* **18,** 445–456
26. Ruddock, L. W., Hirst, T. R., and Freedman, R. B. (1996) *Biochem. J.* **315,** 1001–1005
27. Hansen, R. E., Ostergaard, H., and Winther, J. R. (2005) *Biochemistry* **44,** 5899–5906
28. Sali, A., and Blundell, T. L. (1993) *J. Mol. Biol.* **234,** 779–815
29. Kemmink, J., Darby, N. J., Dijkstra, K., Nilges, M., and Creighton, T. E. (1996) *Biochemistry* **35,** 7684–7691
30. Wang, S., Trumble, W. R., Liao, H., Wesson, C. R., Dunker, A. K., and Kang, C. H. (1998) *Nat. Struct. Biol.* **5,** 476–483
31. Wallner, B., and Elofsson, A. (2003) *Protein Sci.* **12,** 1073–1086
32. Davis, I. W., Murray, L. W., Richardson, J. S., and Richardson, D. C. (2004) *Nucleic Acids Res.* **32,** W615–W619
33. Rost, B., Yachdav, G., and Liu, J. (2004) *Nucleic Acids Res.* **32,** W321–W326
34. Qin, J., Clore, G. M., Kennedy, W. M., Huth, J. R., and Gronenborn, A. M. (1995) *Structure* **3,** 289–297
35. Maeda, K., Hagglund, P., Finnie, C., Svensson, B., and Henriksen, A. (2006) *Structure* **14,** 1701–1710
36. Martin, J. L., Bardwell, J. C., and Kuriyan, J. (1993) *Nature* **365,** 464–468
37. Darby, N. J., and Creighton, T. E. (1995) *Biochemistry* **34,** 16770–16780
38. Raturi, A., and Mutus, B. (2007) *Free Radic. Biol. Med.* **43,** 62–70
39. Alanen, H. I., Salo, K. E., Pekkala, M., Siekkinen, H. M., Pirneskoski, A., and Ruddock, L. W. (2003) *Antioxid. Redox Signal* **5,** 367–374
40. Zapun, A., Bardwell, J. C., and Creighton, T. E. (1993) *Biochemistry* **32,** 5083–5092
41. Mezghrani, A., Fassio, A., Benham, A., Simmen, T., Braakman, I., and Sitia, R. (2001) *EMBO J.* **20,** 6288–6296
42. Lappi, A. K., Lensink, M. F., Alanen, H. I., Salo, K. E., Lobell, M., Juffer, A. H., and Ruddock, L. W. (2004) *J. Mol. Biol.* **335,** 283–295
43. Delano, W. L. (2002) *The PyMOL Molecular Graphics System*, DeLano Scientific, Palo Alto, CA